Electric-field activated variable-range hopping transport in $PrBa_2Cu_3O_{7-\delta}$

G. K. van Ancum, M. A. J. Verhoeven, D. H. A. Blank, and H. Rogalla
Department of Applied Physics, University of Twente, P.O. Box 217, NL-7500 AE Enschede, The Netherlands
(Received 25 January 1995)

We demonstrate the transport of charge carriers in $PrBa_2Cu_3O_{7-\delta}$ (PBCO) to be dependent both on the applied electric field and on the temperature. In our measurements we use inert noble-metal contacts on laser ablated and sputtered PBCO films. By applying the transmission line model we are able to separate the contact resistance from the PBCO resistance. The average hopping distance can be found by extending Mott's formula to field activation, and is found to be much greater than the dimensions of the PBCO unit cell. From the measurements in strong electric field a minimum hopping distance in the direction of the applied field of about 14 nm is determined, which we discuss in terms of localized states and intrinsic mixed valence of the Pr atoms in the PBCO film.

I. INTRODUCTION

The drastic depression of T_c on substituting Y by Pr in $YBa_2Cu_3O_{7-\delta}$ (YBCO) gives rise to a wide discussion in the literature. In contrast to all other rare-earth substitutions for Y (Nd, Sm, Eu, Gd, Dy, Ho, Er, Tm, Yb, and Lu) superconductivity is quenched in $Y_{1-x}Pr_xBa_2Cu_3O_{7-\delta}$ for $x>0.55$, and pure $PrBa_2Cu_3O_{7-\delta}$ (PBCO) exhibits semiconducting behavior. The transition from superconducting YBCO to semiconducting PBCO is still a stumbling block for most theories on high-T_c superconductivity.[1,2] The electrical transport mechanism of PBCO, generally described using a concept of carrier localization, is interesting by itself. At low temperatures carrier localization results in a variable-range hopping (VRH) conduction mechanism, as introduced by Mott.[3] In the classical Mott model the hopping of carriers is temperature activated, yielding a temperature-dependent resistivity. In this paper we include activation by an applied electric field in the description of the transport mechanism of PBCO. In this case the resistivity is dependent on both the electrical field and the temperature.

Resistivity measurements play a key role in the discussion about the different properties of YBCO and PBCO, as well as in the experiments on the transport mechanism of PBCO. Measuring the extremely high resistivity of PBCO thin films at low temperatures (typically $\rho=1-10$ Ω m at $T=10$ K) requires a careful approach. Some authors use superconducting electrodes,[4] thus limiting themselves to temperatures below the critical temperature T_c of their electrodes, and introducing superconducting coupling and pair-breaking effects. These effects could be a source of errors. In our view Ohmic contacts of noble-metal electrodes should be preferred.

The main problem in using noble-metal electrodes is the high contact resistivity between the PBCO and the electrode material, which is additionally strongly temperature dependent. Standard four-point measurement techniques, routinely used on superconducting YBCO, cannot identify errors caused by a very high contact resistance in combination with a high sample resistance. Therefore, we employ the transmission line model[5] (TLM) to separate the contact resistance from the PBCO resistance.

II. FILM PREPARATION

We used two batches of PBCO thin films. One batch was laser ablated on Y-stabilized ZrO_2 substrates with a CeO_2 buffer layer to improve the lattice match and thus the quality of the PBCO film. The other batch was sputter deposited on $SrTiO_3$ substrates. All films have a thickness of 100 nm. Details on the deposition can be found elsewhere.[6,7] The isolation resistance of both types of substrates and the CeO_2 layer was measured to be orders of magnitude larger than the PBCO film resistance.

From x-ray diffraction measurements we conclude that the films are *c*-axis oriented, with the *a*,*b* planes parallel to the substrate. The *c*-axis length corresponds to fully oxygenated films. The laser ablated films show some structure at the surface, whereas the sputtered films are smooth. We analyzed the surface of laser ablated and sputtered films with an atomic force microscope (AFM). From 2×2 μm AFM scans we found a root-mean-square surface roughness of typically 5 nm for laser ablated films, and for sputtered films typically 2 nm.

Using a photoresist mask the largest part of the film is removed by wet chemical etching in H_3PO_4:H_2O solution (1:100), leaving a bar with a length of 2685 μm and a width of 300 μm in the middle of the substrate. On this TLM bar we align a second mask defining contacts using a lift-off step. Prior to the deposition of the contacts the surface of the TLM bar is cleaned *in situ* by etching a few nanometers in an argon plasma, thus removing possible contaminations. The contacts are sputter deposited without an adhesion layer. Their thickness is approximately 60 nm.

The TLM structure consists of eight contacts with lengths of 200 μm, leaving seven stretches of PBCO with lengths of 5, 10, 20, 50, 100, 200, and 500 μm, respectively. The sample is glued to a sample holder with an isolation resistance better than 1 TΩ. Contacts between the

film and the sample holder are made by wire bonding.

The measurements were carried out in a standard flow cryostat. To determine the resistance between two neighboring contacts on the TLM bar, we measure the current I as a function of the applied voltage V. From the IV data the differential resistance is calculated numerically using nine consecutive points.[8]

For the measurements we apply a Keithley Source Measure Unit (SMU). The accuracy of its voltage source is 100 μV, its current meter has a maximum resolution of 5 fA. Three-axial wiring is used from the SMU to the cryostat. A driven guard surrounds the sensitive wire down to the sample holder to prevent leakage currents. The whole insert, including the sample holder, is surrounded by a grounded shield to reduce noise.

Testing the setup without a sample showed that the minimum current is determined by the equipment and not by the leakage resistance of the insert. There is no measurable leakage current from the insert to ground. With the present equipment, resistances up to 1 TΩ can be measured.

III. TRANSMISSION LINE MODEL

The transmission line model was introduced by Berger to study the quality and reliability of planar contacts to monolithic circuits.[5] In this model only one-dimensional (1D) current flow was accounted for. The model was extended later by Pimbly,[9] allowing the current to flow perpendicularly to the contact. For our geometry, with a very thin PBCO film, we use the model as presented by Berger. In the TLM three subsystems are considered: the sheet, the contact, and an interface layer. The contact is assumed to be an equipotential plane. The differential resistance at zero bias voltage $R=\partial V/\partial I$ as a function of the contact spacing L is given by

$$R(L)=\frac{R_s}{W}L+\frac{2R_sL_t}{W}\coth\frac{c}{L_t}\ , \tag{1}$$

where c represents the contact length, W the contact width, R_s the sheet resistance, and L_t the transfer length (see Fig. 1). The transfer length is the length over which 90% of the current is injected into the film. For $c \gg L_t$ the "coth" factor equals 1. Plotting R versus L we determine R_s from the slope, and L_t from the intercept at $L=0$ using a least-squares fit. Applying very thin films, we assume the current to be constant over the thickness of the film. The PBCO resistivity ρ_{PBCO} can then be related to the sheet resistance R_s as

$$\rho_{\mathrm{PBCO}}=R_sd\ , \tag{2}$$

with d the film thickness. The contact resistivity ρ_c is defined by

$$\rho_c=R_sL_t^2\ . \tag{3}$$

The value for L_t can be used as a reliability parameter: when L_t approaches the contact length, the contact resistance dominates the measurement, and the obtained sheet resistance is likely to be prone to errors.

Strictly speaking, the model is only valid for Ohmic contacts. Our contacts on PBCO could be non-Ohmic, e.g., Schottky-barrier-like.[10] However, plotting $R=\partial V/\partial I$ versus the PBCO length L also for nonzero electric field, we were able to show a linear dependence for $L>L_t(0)$, $L_t(0)$ being the zero-field transfer length. The maximum relative error in the slope of the fitted function at $T=11$ K was 13% at $E=2$ kV/m, compared to 4% in zero field.

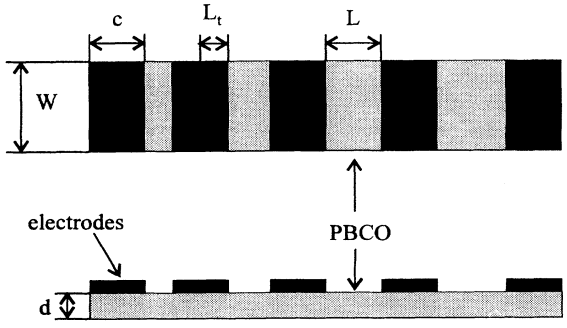

FIG. 1. Layout of the TLM test structure.

IV. CONTACT AND PBCO RESISTIVITY IN ZERO ELECTRIC FIELD

In this section we discuss the contact and the PBCO resistivity in zero electric field. The resistance was determined by taking the derivative from the IV plots at $V=0$ V. Using the TLM we separated the contact resistance from the film resistance. The contact resistivity for gold and silver contacts on laser ablated and sputtered films are presented in Fig. 2. The contact resistivity of silver contacts can be lowered by annealing [15 min in 200 mbar oxygen at 400 °C (Ref. 11)]. For gold contacts we did not see an improvement in the contact resistivity by annealing.

Sputtered films generally show a higher contact resistivity than laser ablated films. For gold contacts the TLM could not be applied at temperatures below $T=80$ K, since the transfer length increased above the contact length. Gold and silver contacts could be used on laser

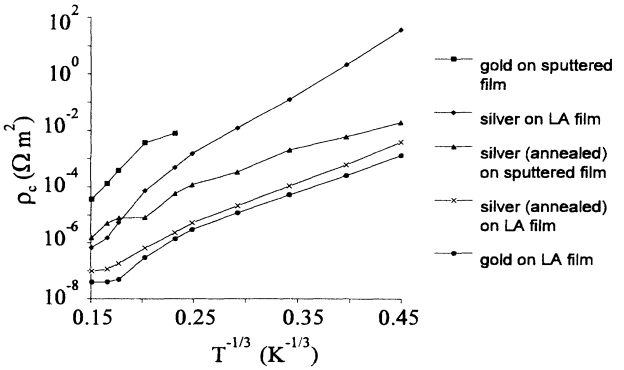

FIG. 2. The contact resistivity ρ_c of gold, silver, and annealed silver contacts on laser ablated films, and of gold and annealed silver contacts on sputtered films.

ablated films, where the gold contacts showed the lowest contact resistivity. The lower contact resistivity on laser ablated films may be due to the rougher surface of these films: AFM measurements revealed a root-mean-square surface roughness of 5 nm, compared to 2 nm for sputtered films.

In Fig. 3 we present the PBCO resistivity in zero electric field, $E=0$ V/m. The rougher surface of the laser ablated films indicates some degree of disorder inside the film, explaining that the laser ablated films have a higher resistivity compared to the sputtered films. Despite the fact that the annealing conditions are identical to the cooling down conditions after deposition of the PBCO film, annealing increased the absolute value of the resistance. The temperature dependence of the PBCO resistivity is the same for laser ablated and sputtered films: the transport processes in both laser ablated and sputtered films are equivalent.

V. FIELD ACTIVATION

The distinction between the 2D and 3D Mott variable-range hopping model is difficult to make on the basis of the available data. To be able to make this distinction clearly, VRH should occur over more decades of temperatures. Unfortunately, this is not the case in our data on PBCO. The problem of differentiating between 2D and 3D behavior was addressed earlier by Fisher *et al.*[12] We checked our data with the 2D and 3D Mott models, and found the different formulas to fit almost equally well. The standard deviations on the slope of the $\ln\rho$ versus $T^{-1/3}$ (2D), and $\ln\rho$ versus $T^{-1/4}$ (3D) plots were 4% and 5%, respectively.

The semilogarithmic plot of ρ_{PBCO} at $E=0$ V/m versus $T^{-1/3}$ (Fig. 3) shows a linear dependence for $T<100$ K, indicating temperature-activated variable-range hopping between localized states.[13] In the classical Mott derivation[3] the hop of a carrier between an initial state and a final state is promoted only by its thermal energy k_BT (with k_B Boltzmann's constant). The electric field can be incorporated in the description of hopping conductivity in different ways. We shall briefly review the proposals found in the literature, and finally present a model that can be used to determine the average hopping distance in the field direction.

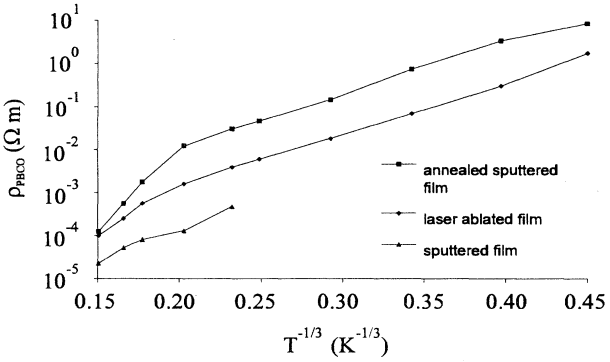

FIG. 3. The PBCO resistivity ρ_{PBCO} for laser ablated and sputtered films in zero electric field.

In the literature on hopping conduction in an electric field, two electric-field regimes are considered separately. The weak-field regime, with $e\varepsilon_r Er \ll k_BT$, and the strong-field regime, where $e\varepsilon_r Er \gg k_BT$, with e the unit of charge, ε_r the relative dielectric constant, r the (average) hopping distance, and E the applied electric field.

Shklovskii[14] assumes nearest-neighbor hopping within an energy bandwidth $e\varepsilon_r Er$, and arrives at $\rho \propto \exp(E^{-1/3})$ in strong electric fields. The model only applies for strong fields, as it neglects temperature activation. In the Apsley and Hughes model[15] the total temperature- and field-dependent conductivity follows by integrating the energy-dependent mobility over the energy. The resistivity is proportional to $\exp(-E^2)$ in weak fields, and to $\exp(E^{-1/3})$ in strong fields. The hopping distance in real space is not addressed by Apsley and Hughes. Pollak and Riess[16] use percolation theory in a mean-field approximation to obtain the conductivity. The localized states are occupied by a time-dependent noninteger average occupation number of charge carriers. As the charge carriers effectively do not move, the average hopping distance cannot be assessed. Pollak and Riess find $\rho \propto \exp(-E)$ in weak fields, and $\rho \propto \exp(E^{-1/3})$ in strong fields. Rentzsch, Schlimak, and Berger[17] apply the model by Pollak and Riess to hopping conductivity in ZnSe films.

As is clear from the above, all models show a $\rho \propto \exp(E^{-1/3})$ dependence for strong electric fields. For weak fields, the different models are not conclusive. In this paper we introduce a model for both weak and strong fields, enabling us to obtain the average hopping distance in the direction of the applied field as a function of the temperature and the electric field. In the limit for strong fields our model yields $\rho \propto \exp(E^{-1/3})$, consistent with the literature.

In an applied electric field the electron gains an energy $e\varepsilon_r Er_x$, with r_x the average hopping distance in the x direction, and E the applied electric field in the x direction. This energy gain can be accounted for in two different ways: first, as effectively decreasing the energy of the final localized state, and second, as an addition to the thermal energy k_BT available to the electron. In the second description temperature and field activation are interchangeable. We include the electric field in the Mott formula as a second activation mechanism, by adding a term $e\varepsilon_r Er_x$ to k_BT:

$$\rho_{\mathrm{PBCO}}(T,E)=\rho_0 \exp\left[\left[\frac{k_BT_0}{k_BT+e\varepsilon_r Er_x(T,E)}\right]^{1/3}\right]. \quad (4)$$

The average hopping distance in the x direction r_x is a function of the applied electric field and the temperature. We can find r_x as a function of the applied field for various temperatures by measuring the resistivity of the PBCO film as a function of temperature *and* field, and fitting these values to Eq. (4).

Figure 4 presents the measured data on the PBCO resistivity: ρ_{PBCO} versus the applied electric field for different temperatures. For temperatures above 100 K temperature activation is dominant, and no field effect can be seen. In this temperature regime nearest-neighbor

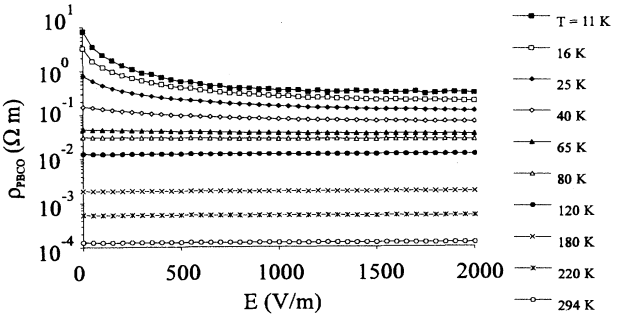

FIG. 4. The PBCO resistivity ρ_{PBCO} vs the applied electric field E for different temperatures.

hopping is likely to be the main transport process. Below $T=100$ K a field dependence is obvious. To obtain information on the average hopping distance we fitted a line through the zero-field points (Fig. 3), yielding ρ_0 and T_0. If we use for ε_r the static dielectric constant $\varepsilon_{dc}\approx 25$,[18] Eq. (4) can be solved, and the average hopping distance in the x direction as a function of the applied field and the temperature can be determined. The results for $r_x(T,E)$ are plotted in Fig. 5.

The average hopping distances in both y and z directions are essentially equal to the zero-field average hopping distance in the x direction, and are not affected by the applied electric field, which acts only in the x direction. For both the 2D and 3D Mott models we calculated the average hopping distance in the field direction with formula (4) or its 3D equivalent. For low activation energies the average hopping distance in the x direction exceeded 100 nm, and thus also the average hopping distance in the z direction exceeds 100 nm independent of the applied field. So, the film dimension in the z direction (i.e., the film thickness of 100 nm) cannot accommodate an average hop in this direction. This argument validates the use of the 2D Mott model.

An increase in the average hopping distance in the x direction implies an increase in the average total hopping distance. Analysis of the data shows that (a) the average hopping distance increases at lower temperatures, and (b) the average hopping distance decreases in higher fields. For weak fields ($E<200$ V/m) the obtained values for r_x are less accurate, as the temperature activation is dominant in this regime. The behavior for $E>200$ V/m can be understood as follows: for low activation energies the electron has to travel (hop) a long way to find a state with an energy that is close enough to its initial energy. On increasing the activation energy by raising the temperature or applying an electric field, the range of accessible energies broadens. More states near the initial state become available to the electron, and the average hopping distance decreases. At low temperatures and in weak fields the small current is carried by a few hops over a long distance. At higher temperatures, and equivalently in higher fields, more current is carried by more hops over a shorter distance.

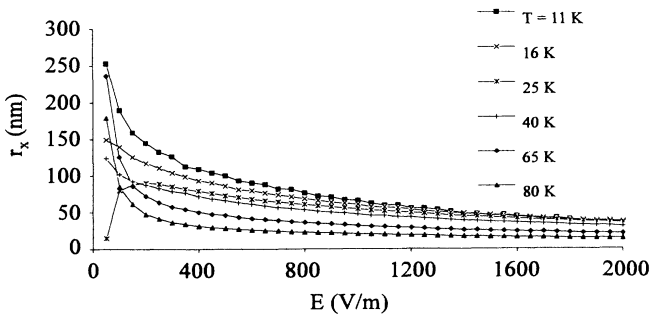

FIG. 5. The average hopping distance in the field direction r_x as a function of the applied electric field E for different temperatures below 80 K.

In high fields the average hopping distance in the x direction tends towards a constant minimum value of approximately 14 nm. We interpret this minimum hopping distance as nearest-neighbor hopping between localized states. The obtained value of 14 nm is comparable to the estimate in the literature for the nearest-neighbor distance $x_{NN}\approx 10$ nm, obtained by fitting the IV curves of a junction with a PBCO barrier.[4]

Another way to explain the field-dependent resistivity would be dissipation in the PBCO film. This would (locally) increase the temperature, and hence lower the resistance. However, the dissipated power in the PBCO thin film is of the order of 40 nW/μm^2. On the basis of the literature on field-effect devices[19] we estimate a maximum temperature rise of 3 mK. Therefore heating cannot explain the observed field dependencies.

VI. CONCLUSION

For thin PBCO films we have demonstrated the resistivity to be dependent on both the external applied electric field and the temperature. We obtained an average hopping distance in the field direction as a function of temperature and field by adding the energy gain due to the applied electric field, $e\varepsilon_r E r_x$, to the thermal energy $k_B T$ in the classical Mott formula. For low activation, i.e., low temperatures and weak fields, the hopping distance is much greater than the dimensions of the PBCO unit cell. By increasing the activation, the average hopping distance in the field direction decreases to approximately 14 nm. The decreasing hopping distance complies with the Mott picture for variable-range hopping.

In our measurements we have used noble-metal electrodes. In order to measure the resistivity of PBCO thin films, we employed the transmission line model to eliminate the influence of the contact resistance. The contact resistivity strongly depends on the surface morphology of the film. Laser ablated films have a higher rms surface roughness, and show a lower contact resistivity compared to smoother sputtered films. The higher surface roughness of the laser ablated films, indicating more disorder in the film, is also reflected in the higher resistivity of laser ablated PBCO films.

The origin of the localization in PBCO, and the role of

the Pr atom in the localization, have been, and are still under discussion.[1,2,20] We note that the nearest-neighbor distances are one to two orders of magnitude greater than the dimensions of the PBCO unit cell ($0.3878 \times 0.3928 \times 1.171$ nm in the *a*, *b*, and *c* directions[20]). If we assume *intrinsic* localized states, this leads us to the conclusion that not all Pr atoms serve as hosts to a localized state. Only an estimated 3% of the Pr atoms provide a localized state. This argument agrees with a mixed valence state of the Pr atoms, where most Pr atoms are in the 3^+ valence state, and only a few Pr atoms in the 4^+ valence state, having a localized hole in their vicinity.

ACKNOWLEDGMENTS

We would like to thank F. J. G. Roesthuis for the pulsed laser deposited films. The AFM measurements on the films were carried out by R. G. Wichern. M. A. J. Doorn took part in the measurements of the contact resistivity.

[1]R. Fehrenbacher and T. M. Rice, Phys. Rev. Lett. **70**, 3471 (1993), and references therein.
[2]D. Khomskii, J. Supercond. **6**, 69 (1993).
[3]N. F. Mott and E. A. Davis, *Electronic Processes in Non-Crystalline Materials* (Clarendon, Oxford, 1979).
[4]U. Kabasawa *et al.*, Phys. Rev. Lett. **70**, 1700 (1993).
[5]H. H. Berger, Solid-State Electron. **15**, 145 (1972).
[6]R. P. J. IJsselstein, Ph.D. thesis, University of Twente, The Netherlands, 1994.
[7]J. Gao, B. Häuser, and H. Rogalla, J. Appl. Phys. **67**, 2512 (1990).
[8]A. Savitzky and M. J. E. Golay, Angew. Chem. **36**, 1627 (1964).
[9]J. M. Pimbley, IEEE Trans. Electron Dev. **ED-33**, 1795 (1986).
[10]See, e.g., D. K. Schroder, *Semiconductor Material and Device Characterization* (Wiley, New York, 1990), Chap. 3.
[11]R. P. Robertazzi *et al.*, Phys. Rev. B **46**, 8456 (1992).
[12]B. Fisher *et al.*, Physica (Amsterdam) **176C**, 75 (1991).
[13]B. I. Shklovskii and A. L. Elfros, *Electron Properties of Doped Semiconductors* (Springer-Verlag, Berlin, 1984), Chap. 9.
[14]B. I. Shklovskii, Fiz. Tekh. Poluprovodn. **6**, 2335 (1972) [Sov. Phys. Semicond. **6**, 1964 (1973)].
[15]N. Apsley and H. P. Hughes, Philos. Mag. **31**, 1327 (1975).
[16]M. Pollak and I. Riess, J. Phys. C **9**, 2339 (1976).
[17]R. Rentzsch, I. S. Shlimak, and H. Berger, Phys. Status Solidi A **54**, 487 (1979).
[18]S. V. Varyukhin and O. E. Parfenov, Pis'ma Zh. Eksp. Teor. Fiz. **58**, 98 (1993) [JETP Lett. **58**, 101 (1993)].
[19]Yu. M. Boguslavskij *et al.*, in *Applied Superconductivity*, edited by H. C. Freyhardt (DGM Informationsgesellschaft mbH, Oberursel, 1993), Vol. 2, p. 1641.
[20]H. B. Radousky, J. Mat. Res. **7**, 1917 (1992).

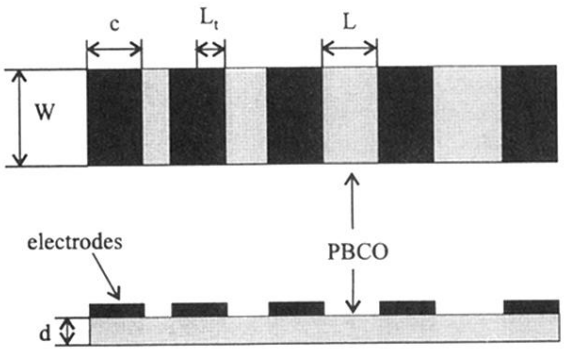

FIG. 1. Layout of the TLM test structure.